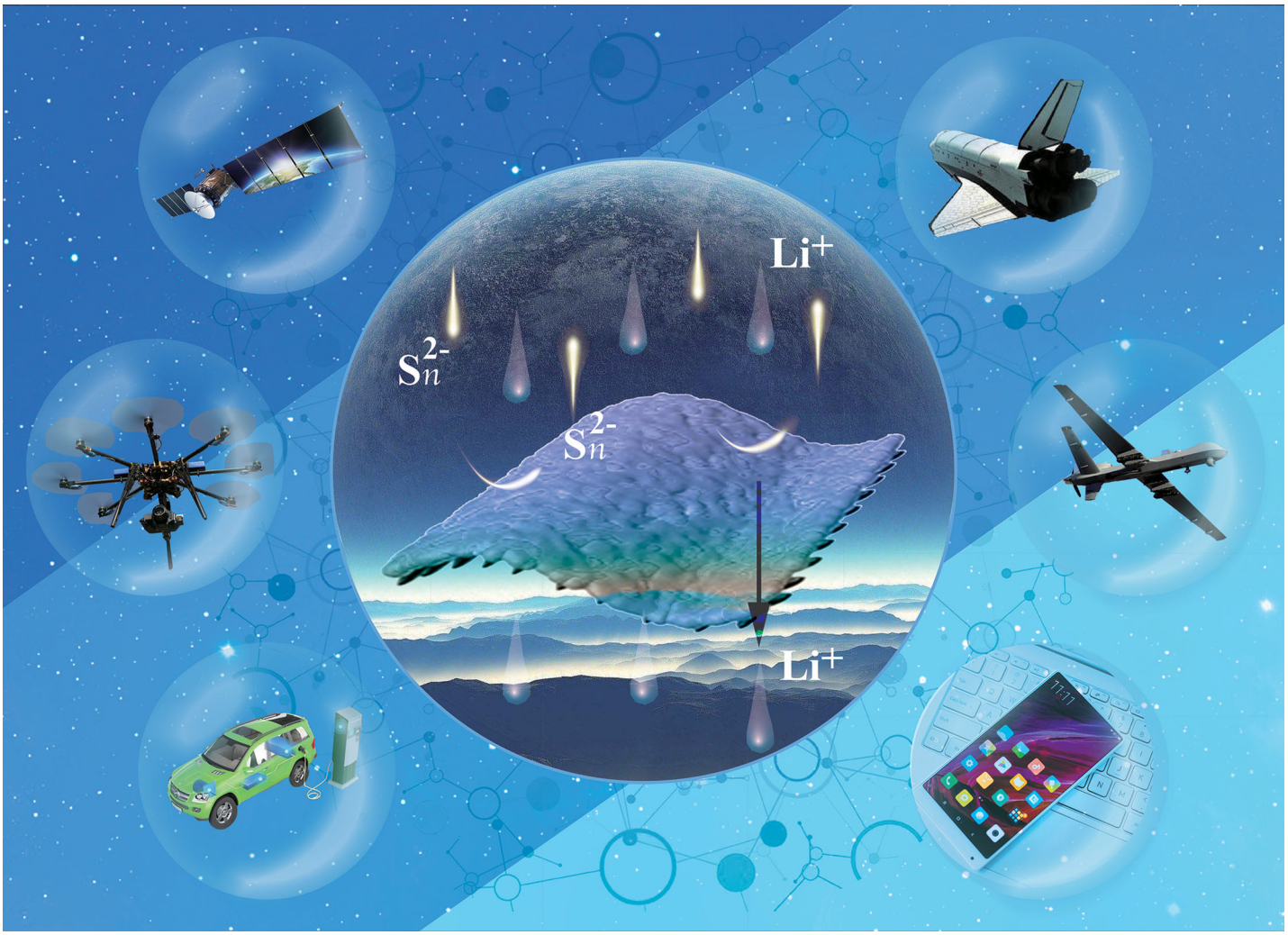

Showcasing research from Nanjing University of Aeronautics and Astronautics, and Massachusetts Institute of Technology.

Ad hoc solid electrolyte on acidized carbon nanotube paper improves cycle life of lithium–sulfur batteries

The *in situ* polymerized solid barrier stops sulfur transport while still allowing bidirectional Li^+ transport, alleviating the shuttle effect and increasing the cycling performance of lithium–sulfur batteries. Such a soft, sticky, hermetic and thin solid electrolyte layer may also find applications for general Li metal protection on the anode side as well.

As featured in:

See Akihiro Kushima, Xiaogang Zhang, Ju Li *et al.*, *Energy Environ. Sci.*, 2017, **10**, 2544.

ROYAL SOCIETY OF CHEMISTRY

rsc.li/ees

Registered charity number: 207890

Energy & Environmental Science

PAPER

View Article Online
View Journal | View Issue

Cite this: *Energy Environ. Sci.*, 2017, **10**, 2544

Ad hoc solid electrolyte on acidized carbon nanotube paper improves cycle life of lithium–sulfur batteries†

Guiyin Xu, [ab] Akihiro Kushima, *[bc] Jiaren Yuan,[a] Hui Dou,[a] Weijiang Xue, [b] Xiaogang Zhang, *[a] Xiaohong Yan[ad] and Ju Li *[b]

Received 7th July 2017,
Accepted 6th September 2017

DOI: 10.1039/c7ee01898c

rsc.li/ees

The performance of lithium–sulfur (Li–S) batteries is greatly improved by using acidized carbon nanotube paper (ACNTP) to induce *in situ* polymerization of ether-based DOL/DME liquid to grow an ion-selective solid barrier, to seal in soluble polysulfides on the cathode side. The Li–S battery with the *in situ* barrier showed an initial specific capacity of 683 mA h g^{-1} at a high current density of 1675 mA g^{-1}, and maintained a discharge capacity of 454 mA h g^{-1} after 400 cycles. The capacity decay rate was 0.1% per cycle and a high Coulombic efficiency of 99% was achieved. Experimental characterizations and theoretical models demonstrate the *in situ* polymerized solid barrier stops sulfur transport while still allowing bidirectional Li^+ transport, alleviating the shuttle effect and increasing the cycling performance. The soft and sticky nature of the solid electrolyte barrier makes it a good sealant, forming an enclosed catholyte chamber on the sulfur side.

Broader context

Lithium–sulfur batteries have higher energy density because they exploit anion-redox reactions of abundant and environmentally friendly sulfur, instead of redox of heavier and more expensive transition-metal cations (Co, Ni). The cycling life can be improved by imposing a barrier between the cathode and the separator to selectively block the diffusion of soluble lithium polysulfides. However, exactly how such barriers work is unclear, because many of these membranes are porous with pore size larger than 2 nm. This leads to a hypothesis that a transport barrier may be established *in situ* due to fouling of the pores by polymerized solvent/salt/polysulfides that form a dense solid deposit. In this work, the performance of Li–S batteries is greatly improved by using acidized carbon nanotube paper to induce *in situ* polymerization of ether-based DOL/DME liquid to grow an ion-selective dense solid electrolyte. We demonstrate that such a soft and sticky solid electrolyte $\sim 10^2$ nm thick serves as a hermetic sealant layer, and is also macroscopically deformable as grown on the back of a flexible mesh. Such soft, sticky, hermetic and thin solid electrolyte layer may find applications for general Li metal protection on the anode side as well.

Compared to lithium ion batteries, lithium–sulfur (Li–S) and lithium–oxygen batteries have potentially higher gravimetric energy density because they exploit anion-redox ($A^{x-} \leftrightarrow A^{y-}$, A = S, O) reactions, instead of redox of much heavier and more expensive transition metal cations ($TM^{x+} \leftrightarrow TM^{y+}$, TM = Co, Ni, *etc.*), as Li^+ gets in and out of the cathode.[1] A common phenomenon in batteries with anion-redox cathodes is shuttling of soluble radicals (such as polysulfides, superoxide anions) in the liquid electrolyte. While shuttling to the anode can be beneficial for fully sealed lithium–"solid oxygen" batteries,[1] it is harmful to the cyclability of lithium–sulfur batteries,[2,3] because if sulfur species can cross over to the anode (which is often lithium metal), it tends to deposit there as solid reaction product and cause permanent capacity loss. What one needs is an ion-selective membrane that stops the transport of sulfur in any valence state, but still allows Li^+ transport. A possible way to fulfill this is just a solid electrolyte membrane. In this paper we show that such a sulfur-stopping, Li-transporting solid electrolyte membrane can be formed naturally as the "fouling product" on an appropriate porous substrate, the acidized carbon nanotube paper (ACNTP), which greatly improves the cyclability of Li–S batteries.

[a] *Jiangsu Key Laboratory of Material and Technology for Energy Conversion, College of Material Science and Engineering, Nanjing University of Aeronautics and Astronautics, Nanjing 210016, China. E-mail: azhangxg@nuaa.edu.cn*
[b] *Department of Nuclear Science and Engineering and Department of Materials Science and Engineering, Massachusetts Institute of Technology, Cambridge, Massachusetts 02139, USA. E-mail: kushima@mit.edu, liju@mit.edu*
[c] *Advanced Materials Processing and Analysis Center, Department of Materials Science and Engineering, University of Central Florida, Orlando, Florida 32816, USA. E-mail: kushima@ucf.edu*
[d] *School of Material Science and Engineering, Jiangsu University, Zhenjiang, 212013, China*

† Electronic supplementary information (ESI) available: Detailed description of the experimental procedures and calculations. See DOI: 10.1039/c7ee01898c

The sulfur cathode has a high theoretical energy density of 2600 W h kg^{-1}.[4–7] Moreover, sulfur is environmentally friendly and very cheap. However, the low electronic conductivity of S and Li_2S can cause sluggish kinetics in Li–S cathode. Second, the soluble intermediate lithium polysulfides, if unimpeded (for example by a sealant), will spontaneously diffuse through the liquid electrolyte and parasitically react with the metal lithium anode, leading to capacity degradation. Last but not least, the safety of Li–S batteries is a concern in practical applications due to lithium corrosion during extended cycling. Various strategies have been proposed to alleviate these problems. A wide range of porous carbon materials have been designed as the host for sulfur,[8–10] which improve the electronic conductivity of the cathode and restrain the dissolution of lithium polysulfides by physical adsorption. However, the bonding between carbon and sulfur is weak,[11] causing initially adsorbed sulfur in preparation to desorb during repeated cycling in the form of lithium polysulfides.

Recently, the cycling performance of Li–S batteries is improved by imposing a barrier between the cathode and the separator to selectively block the diffusion of lithium polysulfides and mitigate the shuttling effect.[12–15] However, exactly how such barriers work is unclear, because many of these membranes are porous with pore size larger than 2 nm, which cannot stop polysulfide molecule diffusion physically. In all the experiments we carried out below, we have used a common liquid electrolyte formulation for Li–S batteries, 1 mol L^{-1} LiTFSI and 0.1 mol L^{-1} $LiNO_3$ in a mixed solvent of 1,3-dioxolane (DOL) and 1,2-dimethoxyethane (DME) with a volume ratio of 1 : 1. It turns out that carbon nanotube paper, sandwiched between two polypropylene (PP) separators, is very effective in reducing polysulfide shuttling and enhancing battery cyclability. This may sound unlikely initially, since the open pores are tens of nanometers across (Fig. 1c), which certainly cannot stop lithium polysulfides (Li_2S_n, $4 \leq n \leq 8$) diffusion directly.

This leads to a hypothesis that a transport barrier may be established *in situ* as a consequence of fouling of the pores, developed by polymerized solvent/salt/polysulfides that form a dense solid deposit. This deposition may already occur partially when the ACNTP first contacted liquid solvent/salt, and further consolidated during battery cycling with the addition of polysulfides. It could be analogous to pouring wet concrete into steel rebar preform to get reinforced concrete floor (Fig. 1a), which after setting, becomes solid and hermetic. The best barrier would be a material that allows fast Li^+ transport but exceptionally slows S transport, so a high $D(Li^+)/D(S)$ ratio is desirable. We know that certain sulfur-containing solids can be excellent Li-ion conductors.[16–19] Also, the Li transference number t_{Li}, which is the relative contribution of Li^+ to total ionic conductivity, tends to be much higher in solid electrolyte than in liquid electrolyte. In common liquid electrolytes, anions usually diffuse faster than Li^+ ($t_{Li} < 0.5$) because the transport of Li^+ in liquid involves the vehicular motion of an entire solvation shell structure surrounding Li^+, not just Li^+ itself. In solids, Li^+ moves by a different mechanism, which is hopping or exchange of the naked Li^+ cation, similar to the "Grotthuss mechanism"[20] of the fast proton conductor. In a compact environment of the solid, Li^+ hopping may still be facile due to the small size of Li^+, but it is impossible for sulfur or sulfur-containing complexes to do the same in solids, unlike in liquids (where after adding the solvation shell, the solvated clusters are similar in size). From above, we hypothesize the best kind of defense against polysulfides would indeed be a solid electrolyte, if it can be made hermetic. This solid electrolyte layer should also have some mechanical flexibility, since the catholyte chamber can sustain significant volume change as Li^+ gets in and out (approximately 15 $Å^3$ per Li)[21] and hermiticity needs to be maintained during cycling.

Therefore in addition to $D(Li^+)$ and $D(S)$, what is also critical is the mechanical property of this "sealant". *A priori*, it is not

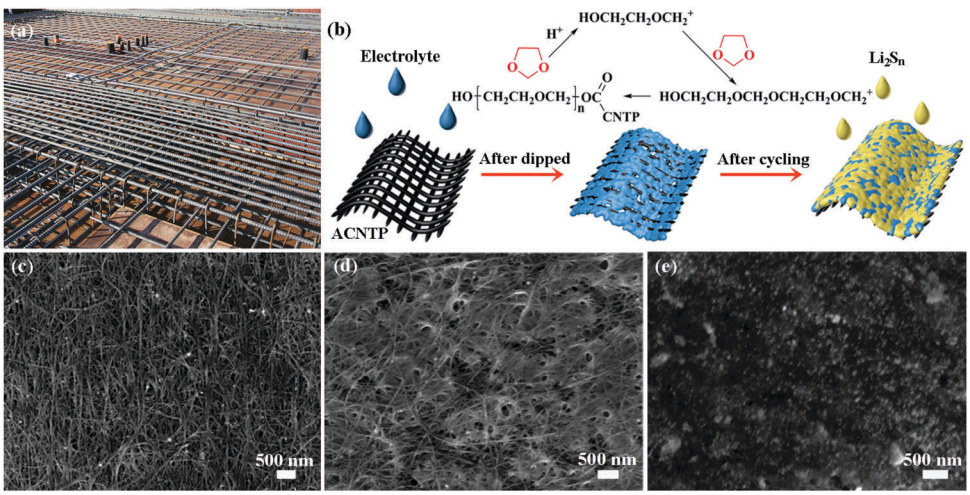

Fig. 1 Schematic illustrations of (a) steel rebar mesh before concrete is poured. After the concrete is poured and set, it will turn into a solid floor. Image taken from https://en.wikipedia.org/wiki/Reinforced_concrete. (b) Illustrations of the process of ACNTP in the electrolyte (The ChemDraw inset is the cationic polymerization of DOL). Scanning electron microscopy (SEM) images of (c) ACNTP before placing into the cell in contact with the electrolyte, (d) ACNTP/*ad hoc* grown solid electrolyte composite, and (e) the cycled ACNTP.

easy to seal up the entire cathode side to become a hermetic chamber containing catholytes, that also needs to withstand the inevitable volume change of the catholyte chamber during cycling. A soft, deformable, sticky and thin solid electrolyte that is also formed *in situ* and therefore self-healing seems to be the best approach, compared to say, rigid ceramics. Carbon nanotube paper (CNTP) has excellent flexibility, electronic conductivity ($\sim 8.0 \times 10^4$ S m^{-1}), thermal conductivity, and mechanical property, and is therefore a good candidate in this regard.

It is known that ether-based liquid electrolyte is prone to polymerization-induced gelation, so small amount of polymerization inhibitors are often added to maintain it in liquid state.[22–24] When the CNTP is treated by HNO_3 and repeatedly washed with water and absolute ethanol, surface groups like O–H and –COOH will be generated (Fig. S1, ESI†), and the proton from –COOH may initiate the cationic polymerization of DOL (the inset in Fig. 1b).[25] This chemically initiated polymerization of the liquid electrolyte may also trap salt and polysulfides to nucleate and grow the *ad hoc* solid electrolyte layer. While such gel has lower Li^+ diffusivity than liquid (the point of adding the polymerization inhibitor), if the gel layer is thin enough, it will not impact the battery performance.

A mass-produced CNTP (purchased from Suzhou Jiedi) is adopted. To understand how the *ad hoc* solid electrolyte is formed, we first dripped liquid electrolyte (without polysulfide) onto the CNTP and ACNTP (left in Fig. 1b), then thoroughly wash it with absolute methanol. There appears to be some solids attached to CNTP (Fig. S4a, ESI†) before washing, but after washing, few solids remain (Fig. S4b, ESI†). This means the solids on CNTP are too few and too fragile to withstand washing. With ACNTP (formed by treating with HNO_3), much more solids formed before washing (middle in Fig. 1b, d and Fig. S4c, ESI†), and they can withstand vigorous washing (Fig. S4d, ESI†). We then inserted sandwiched ACNTP between two porous polypropylene (PP) separators, which were then assembled into coin cell. After cycling (right in Fig. 1b), we took the cell apart and did post-mortem examination. We found there appeared to be a soft solid electrolyte layer grown on ACNTP, shown in Fig. 1e.

To characterize the thickness and deformability of the *ad hoc* solid electrolyte (ASE) layer, we performed local probe mechanical tests. In Fig. 2a (Video S1, ESI†), we pushed in a sharp metal tip from the top of the layer, and then executed a scratching test. When pushing lightly and then dragging the tip, a sharp line is made within the ASE topcoat (middle panel of Fig. 2a), indicating ASE is soft and ductile with large range of plastic deformation. In contrast, when we pushed in the tip deeper, we observed a drastic change in the scratching behavior: it sank into the original carbon nanotube (CNT) fabric, and then a large sliding resistance was incurred when dragging the tip due to entanglement with the fibers, that eventually resulted in the serrated tearing of the CNT fabric beneath. The entanglement was so strong that the metal tip ended up bent before extraction (Video S1, ESI†). This contrast in sliding resistance gives us a handle on the thickness of the ASE layer, which we estimate to be around $d_{ASE} \sim 100$ nm laying on top of the ACNTP. Such thickness is a reasonable range for the ASE barrier, because compared to the commercial PP separator thickness $d_{separator} \sim 25$ μm, assuming our solid electrolyte has the same room-temperature Li^+ diffusivity as $Li_{10}GeP_2S_{12}$ (LGPS), we should satisfy

$$D_{ASE}(Li^+)c_{ASE}(Li^+)/d_{ASE} \gg D_{separator}(Li^+)c_{separator}(Li^+)/d_{separator} \quad (1)$$

where c is the average concentration, and D is the average diffusivity of the two media. Eqn (1) just says that a good ASE layer should not add much more additional Li^+ transport impedance to the battery than the liquid electrolyte inundated separator. On the other hand, we should have

$$d_{ASE}^2/D_{ASE}(S) \ll \text{Use Life} \quad (2)$$

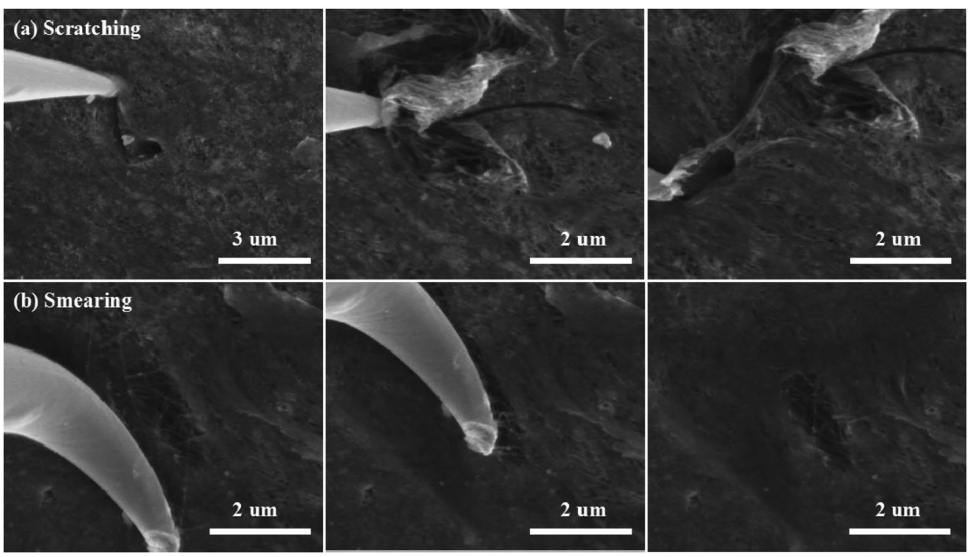

Fig. 2 (a) Scratching test of the *ad hoc* grown solid electrolyte (see Video S1, ESI†) by a nano-manipulator tip in SEM. (b) Smearing test of the same *ad hoc* grown solid electrolyte (see Video S2, ESI†) by a nano-manipulator tip at a different location.

so that sulfur cross-over to the anode should be small over the life of the Li–S battery. Eqn (1) and (2) need to be satisfied simultaneously to be a good polysulfide-stopping ASE layer. This means that while ACNTP initiates the polymerization by surface O–H and –COOH, the polymerization should best be self-limiting, so d_{ASE} does not get too thick. Electrochemical impedance spectroscopy (EIS) of two-layer polypropylene separator (PP + PP), with the ACNTP barrier or the cycled ACNTP barrier placed in between (PP + ACNTP + PP, PP + cycled ACNTP + PP) was measured in H-type cell (Fig. S5, ESI†). The difference in the impedance spectra of PP + PP, PP + ACNTP + PP, and PP + cycled ACNTP + PP is small, indicating that the additional resistance to Li^+ from ASE layer is small compared to the liquid. This result affirms eqn (1) and means that the ASE/ACNTP did not add much additional Li^+ transport impedance. With regard to eqn (2), we will test it through long-term battery cycling and post-mortem analysis.

In Fig. 2b (Video S2, ESI†), we show mechanical smearing of the ASE layer by the already-bent SEM probe, now laying flat on the surface like a spatula. Initially, a hole is made on the ASE, underneath which we see the original porous structure of the carbon nanotube paper that appears largely intact, with still huge and open pores. Then, as we dragged the bent broad tip, we see the ASE smearing over like Silly Putty, and also forming a ''snow bank'' impression on the lower left. It is seen that the ASE is soft, deformable and sticky, making it a good sealant. Because ASE coats on top of a flexible paper with excess area (''give''), ASE backed by ACNTP (ASE/ACNTP) can accommodate large volume change like a wrinkled paper ball. Because it was formed *in situ*, ASE should also have self-healing ability, which allows one to seal-in the catholyte liquid on the cathode side of the cell, despite volume changes generated by cycling and occasional breakages.

CR2016-type coin cells were assembled to evaluate the electrochemical performance of sandwich-structured Li–S batteries. Commercial activated carbon (AC) was used as the sulfur host for its high specific surface area (1964.8 $m^2\ g^{-1}$) and large pore volume (0.91 $cm^3\ g^{-1}$).[26] Transmission electron microscopy (TEM) images and corresponding elemental mapping images of AC/S demonstrate sulfur is uniformly dispersed in AC (Fig. S6, ESI†). The sulfur content in the AC/S composite is 70 wt% (Fig. S7, ESI†). CV curves of Li–S batteries with the ACNTP barrier clearly exhibit a feature of the sulfur oxidation–reduction reaction (Fig. 3a).[27] The stable cathodic peaks at 2.3 and 2.0 V correspond to the anion-reduction reaction of S_8 to Li_2S_n ($4 \leq n \leq 8$) and Li_2S_n to Li_2S_2/Li_2S, respectively. And the anodic peaks at 2.3 and 2.4 V are ascribed to the anion-oxidation reaction of Li_2S/Li_2S_2 to Li_2S_n and Li_2S_n to S_8, respectively. The stable CV peak currents, potentials and areas indicate relatively good reaction reversibility and capacity retention. The galvanostatic charge/discharge curves of AC/S composite electrode, AC/S composite electrode with the CNTP barrier, and AC/S composite electrode with the ACNTP barrier at a constant rate of 0.5C (1C ≡ 1675 mA g^{-1}) show two plateaus in all of the discharge curves (Fig. 3b), which agree well with the CV curves.

The AC/S cathode showed a high initial discharge capacity of 977 mA h g^{-1} at 0.5C due to the excellent electronic conductivity and unique pore-size distribution of AC (''Pure'' in Fig. 3c). However, lithium polysulfides inevitably dissolve into the liquid electrolyte and diffuse to the opposite electrode during repeated cycles because of the weak binding force between AC and sulfur, resulting in the poor cycling performance. The specific capacity decreased ~50% after the first 10 cycles and further to 205 mA h g^{-1} after 250 cycles. On the other hand, the AC/S composite electrode with the CNTP barrier showed an initial specific capacity of 1028 mA h g^{-1} at 0.5C and a high discharge capacity of 569 mA h g^{-1} at the 250th cycle. The capacity decay rate was 0.2% per cycle (''CNTP'' in Fig. 3c). The CNTP barrier physically intercepts and confines the dissolved lithium polysulfides in the cathode side preventing their migrating to the anode side. The resulting highly concentrated lithium polysulfides in cathode region have the common-ion effect to inhibit the further dissolution of sulfur species from the AC/S cathode, decreasing active material loss and alleviating shuttle effect.[28,29] Further improvement was achieved by using ACNTP with an initial specific capacity of 1040 mA h g^{-1} at 0.5C and a high remaining discharge capacity of 674 mA h g^{-1} at the 250th cycle. The capacity decay rate was only 0.1% per cycle (''ACNTP'' in Fig. 3c). Even at 1C, AC/S cathode with the ACNTP barrier showed a specific capacity of 683 mA h g^{-1} in the 1st cycle, and a high discharge capacity of 454 mA h g^{-1} over prolonged 400 cycles with a capacity decay rate of 0.1% per cycle, as well as a high Coulombic efficiency of 99% (Fig. 3d). AC/S cathode with the ACNTP barrier exhibited a good rate performance of 1285 mA h g^{-1} at 0.1C, 1003 mA h g^{-1} at 0.2C, 869 mA h g^{-1} at 0.5C, 756 mA h g^{-1} at 1C, and 660 mA h g^{-1} at 2C. The discharge capacity still recovered to 1030 mA h g^{-1} when the current density fell back to 0.1C (Fig. S8, ESI†).

ACNTP consists of cross-linked carbon nanotube and mainly contains carbon and oxygen (Fig. 4a and Fig. S9a–c, ESI†). Both CNTP and ACNTP barriers can absorb lithium polysulfides. To confirm the adsorption, CV tests were performed for CNTP and ACNTP removed from the coin cell after 50 cycles. The CNTP and ACNTP were used as cathode with Li metal anode in the tests. The CV curves exhibit typical sulfur characteristics at a scan rate of 0.25 mV s^{-1}, demonstrating that CNTP and ACNTP barriers can trap lithium polysulfides (Fig. S10, ESI†). When the CNTP and ACNTP barriers are filled with electrolyte and lithium polysulfides, it is difficult for lithium polysulfides to diffuse through the ''dirty'' barriers. Therefore, stable electrochemical performance was observed after 25 cycles in Fig. 3c. The ACNTP barrier still maintained its flexibility after 250 cycles at 0.5C (Fig. S3, ESI†). Carbon, oxygen, sulfur, and fluorine were detected by the EDS characterization (Fig. S9e–h, ESI†), further confirming the ACNTP barrier effectively intercepted the dissolved lithium polysulfides to the anode. A high sulfur concentration was detected at the small particle shown in III of Fig. 4b and e, demonstrating that lithium polysulfides were captured in the ACNTP cross-section. The ACNTP barrier trapped more lithium polysulfides than the CNTP barrier, as demonstrated by the higher sulfur content in the similar areas of ACNTP than CNTP barrier (Fig. 4b, Fig. S11b, Tables S1 and S2, ESI†). XPS analysis of the cycled ACNTP barrier was performed to detect the

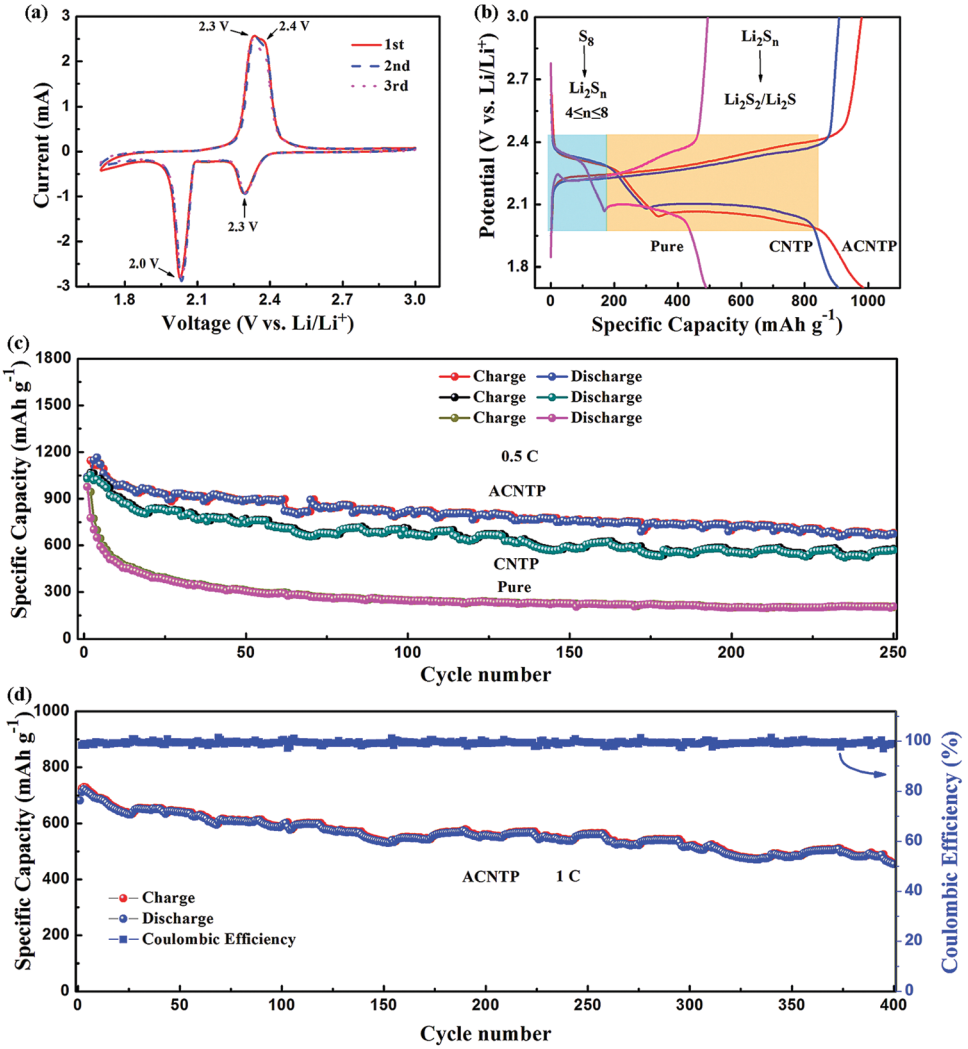

Fig. 3 (a) Typical cyclic voltammetry (CV) curves of AC/S composite electrode with the ACNTP barrier at a scan rate of 0.2 mV s^{-1}. (b) The galvanostatic charge/discharge profiles of the 10th cycle and cycling performance of AC/S composite electrode, AC/S composite electrode with the CNTP barrier, and AC/S composite electrode with the ACNTP barrier at a constant rate of (c) 0.5C and (d) 1C.

carbon, oxygen and sulfur bonds (Fig. S12, ESI†). The C 1s spectra were similar to that of the fresh ACNTP barrier. In the O 1s spectra, the peak at 532.5 eV corresponds to the C═O bonding overlaid with the Li–O bonding.[30] In the S 2p spectra, the peaks at 169.6 and 168.8 eV are attributed to the S–O bonding, which originates from the residual LiTFSI.[31] The other peaks at ~166.8 and ~164.2 eV correspond to the S–S and Li–S bonds from lithium polysulfides, respectively. These results demonstrate the exceptional ability of ACNTP barrier to absorb lithium polysulfides during the battery operation.

To further analyze the acidification effect on the ability to trap lithium polysulfides, the structure and the stability of Li_2S_n (n = 4, 2 and 1) on CNTP and ACNTP were investigated by density functional theory (DFT) calculation. CNTP was modeled as a graphene fragment with a hydrogenated edge (Fig. S13a, ESI†). The adsorption energies of Li_2S_n (n = 4, 2 and 1) trapped on CNTP are −0.18, −0.50 and −0.68 eV, respectively. The O–H and –COOH groups were introduced onto the surface of the CNTP model to simulate the ACNTP (Fig. 4g and k). As shown in Fig. 4, these groups provide perfect adsorption sites and form strong O–Li chemical bonds (ranging 1.86–1.91 Å) with lithium polysulfides. The adsorption energies of Li_2S_n (n = 4, 2 and 1) grafted on –COOH group were −0.98, −0.76 and −0.82 eV, respectively (Fig. 4h–j). When Li_2S_n (n = 4, 2 and 1) was adsorbed to the O–H group, the adsorption energies were −0.73, −0.89 and −0.96 eV, respectively (Fig. 4l–n). The interactions between lithium polysulfides and ACNTP were enhanced compared with those of CNTP (Fig. S13b–d, ESI†). Thus, ACNTP can effectively prevent the discharge products from migrating to the lithium anode. The differential charge densities around Li_2S_n were calculated from the difference of the Li_2S_n-ACNTP charge density and the sum of the Li_2S_n and ACNTP charge density. The red, yellow and green balls represent the O, S, and Li atoms, respectively (the insets in Fig. 4h–j and l–n). The blue isosurface represents electron depletion zones, and the yellow one denotes electron accumulation

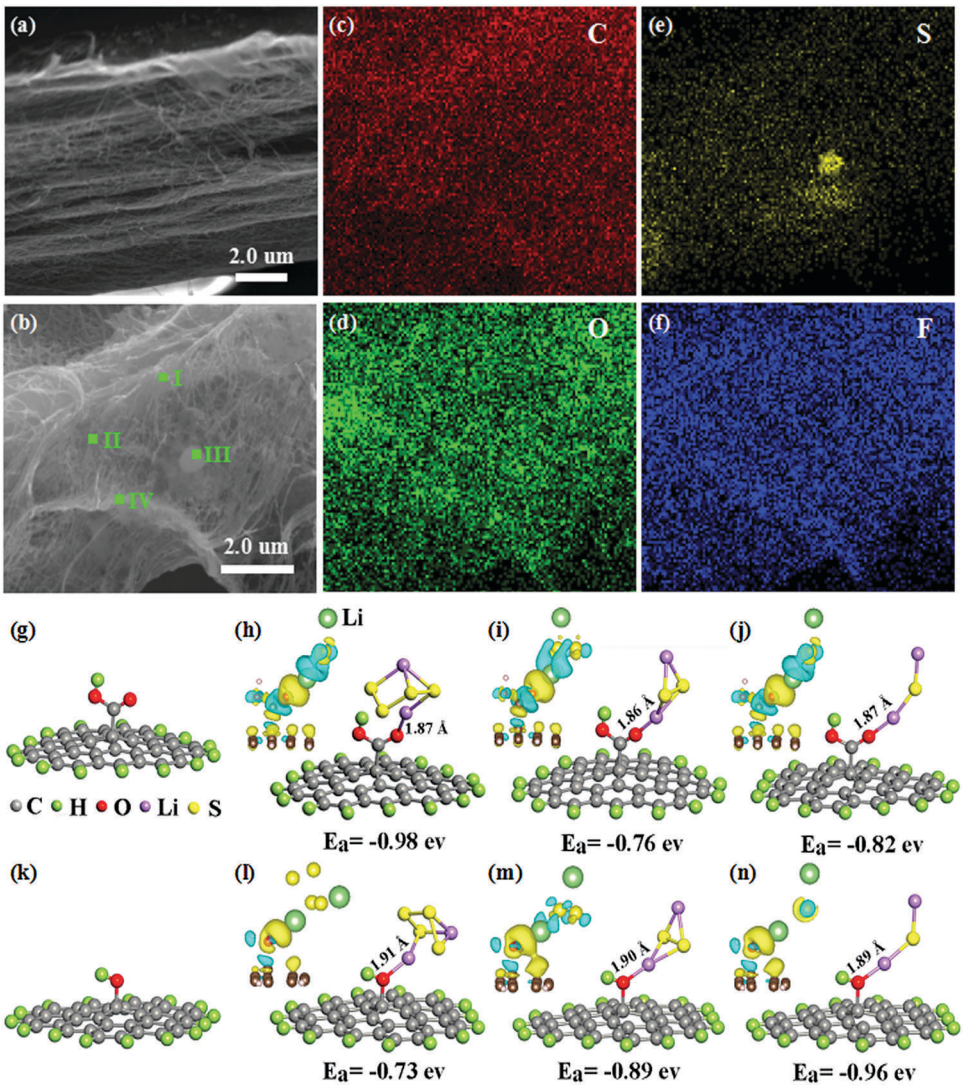

Fig. 4 (a) Scanning electron microscopy (SEM) image of ACNTP cross-section. SEM and energy-dispersive X-ray spectroscopy (EDS) characterization of ACNTP after 50 cycles at 0.5C (charged state): (b) SEM image of the cycled ACNTP. (c–f) EDS elemental maps for the region shown in (b): (c) carbon, (d) oxygen, (e) sulfur and (f) fluorine. The representative geometries after fully optimized show the interactions between (g and k) the ACNTP surface and (h–j and l–n) the Li_2S_n (n = 1, 2, 4) molecules. The insets in (h–j) and (l–n) are the differential charge densities of ACNTP with Li_2S_n.

zones. The electrons accumulate between the Li and O atoms, implying Li atoms bond with O atoms.

There are large spaces between carbon nanotubes in ACNTP (Fig. 5a). After several cycles, the spaces of ACNTP were filled to form a dense solid Li-ion conductor membrane that confined the catholyte (liquid electrolyte with soluble lithium polysulfides) on the cathode side, with large transference number of Li-ion to sulfur diffusivities (Fig. 5b). The covered film on ACNTP consisted of amorphous particles (Fig. 5c). XRD patterns also show no clear peaks from crystal species in the cycled ACNTP (Fig. S14, ESI†). The XRD analysis together with SEM and TEM observations indicates that there exist amorphous-like solid deposits (possibly a mixture of lithium salt and lithium polysulfides) on ACNTP after cycling. This mixture may act as a lithium ion conductor while suppressing the lithium polysulfide diffusion. We conducted *ab initio* molecular dynamics simulation to evaluate the Li and the polysulfide conductivity (see Methodes for the detail). The simulation model used in this simulation is shown in Fig. 5d. Based on F : S ratio in the ACNTP after cycling (Table S2, ESI†), 14 Li^+, 14 $TFSI^-$, and 1 Li_2S_4 molecules were randomly distributed in the simulation box. After the structural optimization, we obtained a simulation box with the size of 13.2 × 13.3 × 13.5 Å corresponding to 2.9 g cm^{-3}. The molecular dynamics simulation was performed at 298 K (Video S3, ESI†). While Li ions diffused freely between $TFSI^-$ networks, Li_2S_4 molecule was trapped and immobile. The calculated mean square displacement (MSD) for Li and S atoms in Li_2S_4 as a function of time is shown in Fig. 5e. From the data we obtained the diffusion constant D_{Li} and $D_{Li_2S_4}$ as 1.4 × 10^{-9} m^2 s^{-1} and 0.33 × 10^{-9} m^2 s^{-1}, respectively. The slower diffusivity and the high adsorption energy of the polysulfide molecule to ACNTP in simulations qualitatively support the polysulfide trapping

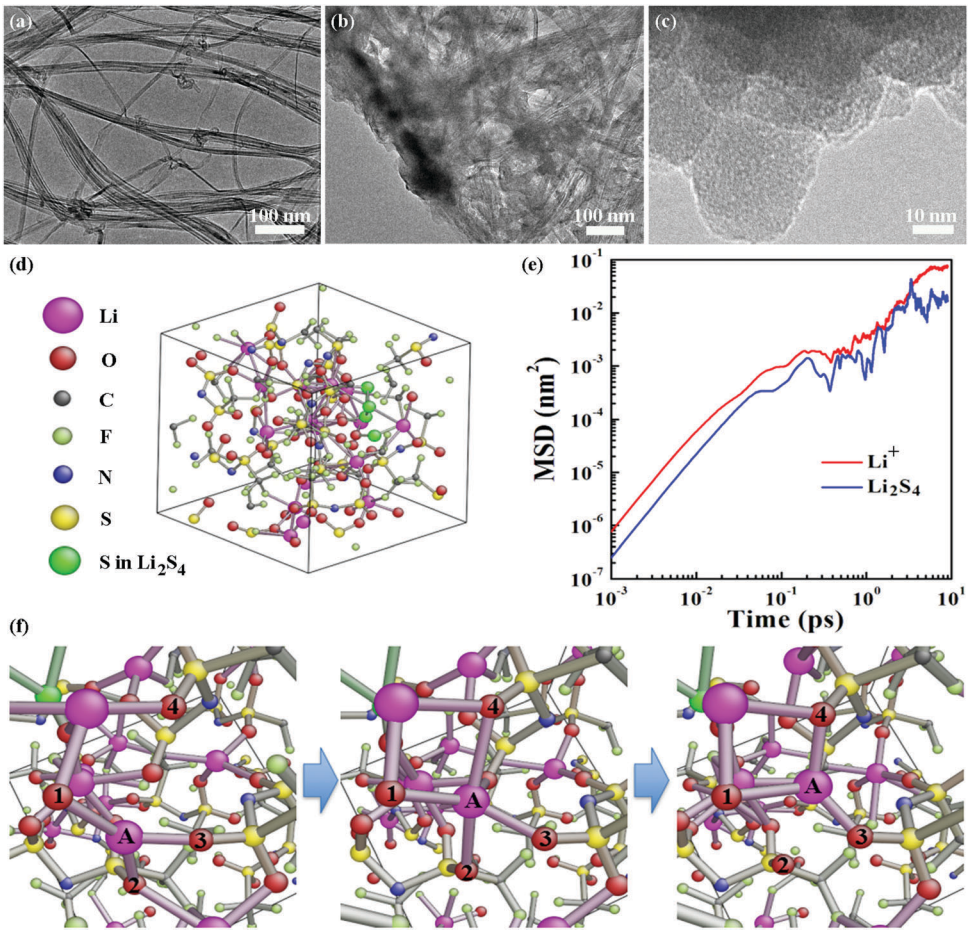

Fig. 5 Transmission electron microscopy (TEM) images of (a) ACNTP and (b and c) cycled ACNTP. (d) Simulation model of the LiTFSI/Li_2S_4 mixture. (e) Mean square displacement (MSD) as a function of time. (f) Li hopping between $TFSI^-$ molecules in the diffusion process.

ability of ASE/ACNTP. Although the D_{Li} is only ~4 times larger than $D_{Li_2S_4}$ initially, the trapping and polymerization initiator effect of ACNTP may trigger a self-reinforcing process (fouling) that further reduces $D(S)/D(Li^+)$.

The Li^+ conductivity σ in the mixture was estimated by Nernst–Einstein relation, $\sigma_i = cq^2D/k_BT$. Here, c is the ion concentration and q is the charge of the ion. The obtained value σ_i = 0.58 S cm^{-1} is extremely high (higher than the best Li ion conducting solid electrolyte reported[32]). Snapshots of the typical Li^+ diffusion process are shown in Fig. 5f. First, Li atom (marked as A) was shared by three $TFSI^-$ molecules with O atoms 1–3. Next, the Li atom shifted towards O atom 4 of another $TFSI^-$. Finally, the Li atom was separated from O atom 2 and became neighbor with O atoms 1, 3, and 4. This bond switching of Li ion between $TFSI^-$ molecules is similar to the "Grotthuss mechanism"[20] of the fast proton transport in water, and contributes to the high ionic conductivity in the lithium salt/polysulfide mixture.

In summary, an ion-selective membrane for Li–S batteries was successfully obtained by a simple acid treatment process. The ACNTP membrane promotes the formation an *ad hoc* solid electrolyte layer topcoat, which is also mechanically flexible, self-sealing and seal-healing. The electrochemical tests demonstrated Li–S batteries with the *in situ* polymerized solid barrier had an excellent capacity retention and high Coulombic efficiency, due to a well-defined catholyte chamber on the sulfur side. The chemical interactions between ACNTP and lithium polysulfides were investigated by DFT. This work demonstrates that a soft solid electrolyte of ~10^2 nm thickness can serve as a hermetic sealant layer, and is also macroscopically deformable when grown on the back of a structurally sound and mechanically flexible mesh or paper (due to wrinkles and excess area). Such mechanically flexible and conforming solid electrolyte layer may find applications not only in Li–S batteries (to define a catholyte chamber), but also for general Li metal protection on the anode side, since large volume variation and conforming soft contact are required there as well.

Conflicts of interest

There are no conflicts to declare.

Acknowledgements

This work is supported by National Key Basic Research Program 973 (2014CB239701), National Natural Science Foundation of

China (51372116), and Natural Science Foundation of Jiangsu Province (BK20151468). G. X. would like to thank Funding of Jiangsu Innovation Program for Graduate Education (KYLX15_0300). J. L. and W. X. acknowledge the support by NSF ECCS-1610806 and Samsung. This work made use of the MRSEC Shared Experimental Facilities at MIT, supported by the National Science Foundation under award number DMR-1419807.

References

1 Z. Zhu, A. Kushima, Z. Yin, L. Qi, K. Amine, J. Lu and J. Li, *Nat. Energy*, 2016, **1**, 16111.
2 Z. Li, J. T. Zhang, Y. M. Chen, J. Li and X. W. Lou, *Nat. Commun.*, 2015, **6**, 8850.
3 J. Niu, A. Kushima, M. Li, Z. Wang, W. Li, C. Wang and J. Li, *J. Mater. Chem. A*, 2014, **2**, 19788–19796.
4 C. Tang, Q. Zhang, M. Q. Zhao, J. Q. Huang, X. B. Cheng, G. L. Tian, H. J. Peng and F. Wei, *Adv. Mater.*, 2014, **26**, 6100–6105.
5 H. Kim, J. T. Lee, A. Magasinski, K. Zhao, Y. Liu and G. Yushin, *Adv. Energy Mater.*, 2015, **5**, 1501306.
6 C. Wang, X. Wang, Y. Yang, A. Kushima, J. Chen, Y. Huang and J. Li, *Nano Lett.*, 2015, **15**, 1796–1802.
7 D. R. MacFarlane, M. Forsyth, P. C. Howlett, M. Kar, S. Passerini, J. M. Pringle, H. Ohno, M. Watanabe, F. Yan, W. Zheng, S. Zhang and J. Zhang, *Nat. Rev. Mater.*, 2016, **1**, 15005.
8 X. Ji, K. T. Lee and L. F. Nazar, *Nat. Mater.*, 2009, **8**, 500–506.
9 N. Jayaprakash, J. Shen, S. S. Moganty, A. Corona and L. A. Archer, *Angew. Chem., Int. Ed.*, 2011, **50**, 5904–5908.
10 M. Oschatz, L. Borchardt, K. Pinkert, S. Thieme, M. R. Lohe, C. Hoffmann, M. Benusch, F. M. Wisser, C. Ziegler, L. Giebeler, M. H. Rümmeli, J. Eckert, A. Eychmüller and S. Kaskel, *Adv. Energy Mater.*, 2014, **4**, 1300645.
11 W. Zhou, X. Xiao, M. Cai and L. Yang, *Nano Lett.*, 2014, **14**, 5250–5256.
12 Y. S. Su and A. Manthiram, *Nat. Commun.*, 2012, **3**, 1166.
13 S. H. Chung and A. Manthiram, *ChemSusChem*, 2014, **7**, 1655–1661.
14 L. Wang, J. Liu, S. Haller, Y. Wang and Y. Xia, *Chem. Commun.*, 2015, **51**, 6996–6999.
15 S. H. Chung, C. H. Chang and A. Manthiram, *Small*, 2015, **12**, 939–950.
16 Z. Liu, W. Fu, E. A. Payzant, X. Yu, Z. Wu, N. J. Dudney, J. Kiggans, K. Hong, A. J. Rondinone and C. Liang, *J. Am. Chem. Soc.*, 2013, **135**, 975–978.
17 T. Ohtomo, A. Hayashi, M. Tatsumisago, Y. Tsuchida, S. Hama and K. Kawamoto, *J. Power Sources*, 2013, **233**, 231–235.
18 M. Nagao, Y. Imade, H. Narisawa, R. Watanabe, T. Yokoi, T. Tatsumi and R. Kanno, *J. Power Sources*, 2013, **243**, 60–64.
19 Y. Wang, W. D. Richards, S. P. Ong, L. J. Miara, J. C. Kim, Y. Mo and G. Ceder, *Nat. Mater.*, 2015, **14**, 1026–1031.
20 C. De Grotthuss, *Mémoire sur la décomposition de l'eau: et des corps qu'elle tient en dissolution à l'aide de l'électricité galvanique*, 1805.
21 S. Kim, S. J. Choi, K. Zhao, H. Yang, G. Gobbi, S. Zhang and J. Li, *Nat. Commun.*, 2016, **7**, 10146.
22 A. Dey and B. P. Sullivan, *Mixed solvents for high and low temperature organic electrolyte batteries*, *US Pat.*, No. 3947289, 1976.
23 B. M. Rao, D. J. Eustace and D. Farcasiu, *Compositions for stabilizing electrolytes in Li/TiS_2 systems, US Pat.*, No. 4284692, 1981.
24 P. R. Moses, A. H. Taylor and M. J. Turchan, *Non-aqueous Li/MnO_2 cell, US Pat.*, No. 4401735, 1983.
25 M. Okada, Y. Yamashita and Y. Ishii, *Die Makromolekulare Chemie*, 1964, **80**, 196–207.
26 G. Xu, J. Yuan, X. Tao, B. Ding, H. Dou, X. Yan, Y. Xiao and X. Zhang, *Nano Res.*, 2015, **8**, 3066–3074.
27 R. Xu, J. Lu and K. Amine, *Adv. Energy Mater.*, 2015, **5**, 1500408.
28 R. Xu, I. Belharouak, J. C. M. Li, X. Zhang, I. Bloom and J. Bareño, *Adv. Energy Mater.*, 2013, **3**, 833–838.
29 L. Miao, W. Wang, K. Yuan, Y. Yang and A. Wang, *Chem. Commun.*, 2014, **50**, 13231–13234.
30 S. Xiong, K. Xie, Y. Diao and X. Hong, *Electrochim. Acta*, 2012, **83**, 78–86.
31 X. Tao, J. Wang, Z. Ying, Q. Cai, G. Zheng, Y. Gan, H. Huang, Y. Xia, C. Liang, W. Zhang and Y. Cui, *Nano Lett.*, 2014, **14**, 5288–5294.
32 N. Kamaya, K. Homma, Y. Yamakawa, M. Hirayama, R. Kanno, M. Yonemura, T. Kamiyama, Y. Kato, S. Hama, K. Kawamoto and A. Mitsui, *Nat. Mater.*, 2011, **10**, 682–686.

Supporting Information

Ad hoc Solid Electrolyte on Acidized Carbon Nanotube Paper Improves Cycle Life of Lithium-Sulfur Batteries

Guiyin Xu,[1,2] Akihiro Kushima,[2,*] Jiaren Yuan,[1] Hui Dou,[1] Weijiang Xue,[2] Xiaogang Zhang,[1,*] Xiaohong Yan,[3] Ju Li[2,*]

[1]Jiangsu Key Laboratory of Material and Technology for Energy Conversion, College of Material Science and Engineering, Nanjing University of Aeronautics and Astronautics, Nanjing 210016, China

[2]Department of Nuclear Science and Engineering and Department of Materials Science and Engineering, Massachusetts Institute of Technology, Cambridge, Massachusetts 02139, USA

[3]School of Material Science and Engineering, Jiangsu University, Zhenjiang, 212013, China

Experimental Procedures

Preparation of ACNTP and the AC/S composite

Carbon nanotubes paper (CNTP) was punched into discs with a diameter of 1.88 cm. Then, the CNTP discs were treated by backflow in 6 mol L^{-1} HNO_3 aqueous solution at 90 °C for 10 h. Then, acidized carbon nanotube paper (ACNTP) was repeatedly washed with water and absolute ethanol. Finally, ACNTP was dried at 60 °C for 12 h.

The AC/S composite was prepared by the mixture of AC (Fuzhou Yihuan Carbon Co. Ltd., China) and sulfur with the mass ratio of 7:3 and heated at 155 °C for 10 h.

Characterization

X-ray diffraction (XRD) patterns were measured on a Bruker-AXS D8 DISCOVER. Copper Kα line was used as a radiation source with λ =0.15406 nm. The X-ray photoelectron spectroscopy (XPS) analysis was performed on a Perkin-Elmer PHI 550 spectrometer with Al Kα (1486.6 eV) as the X-ray source. Field emission scanning electron microscopy (FESEM) and transmission electron microscopy (TEM) measurements were carried out with JEOL JSM-6380LV FE-SEM and FEI TECNAI-20, respectively. Scanning transmission electronic microscope (STEM) was performed on a Tecnai G2 F30. Thermal gravimetric (TG) analysis was conducted on a TG-DSC instrument (NETZSCH STA 409 PC) under a N_2 atmosphere at a heating rate of 10 °C min^{-1} from 30 to 500 °C.

Electrochemical characterization

Electrochemical characterization of the AC/S composite electrode, AC/S composite electrode with the CNTP barrier, and AC/S composite electrode with the ACNTP barrier was carried out by galvanostatic cycling using CR2016-type coin cells. The working electrodes were prepared by a slurry coating procedure. The slurry consisted of 70 wt% active material, 20 wt% acetylene black and 10 wt% polyvinylidene fluoride (PVDF) dissolved in N-methyl pyrrolidinone (NMP), and was uniformly spread on an aluminium foil current collector. Finally, the electrode was dried at 70 °C overnight. Each current collector contained *ca* 2.0 mg cm^{-2} active material (with *ca* 1.0 mg cm^{-2} S). Test cells were assembled in an argon-filled glove box using Li foil as the counter electrode and two-layer polypropylene (PP) film as the separator. The CNTP barrier or the ACNTP barrier is placed between the two-layer separator. The electrolyte was 1 mol L^{-1} LiTFSI and 0.1 mol L^{-1} $LiNO_3$ in a mixed solvent of 1, 3-dioxolane (DOL) and 1, 2-dimethoxyethane (DME) with a volume ratio of 1:1. The coin cells were galvanostatically charged-discharged at different current densities between 1.7 and 3.0 V (*vs.* Li/Li^+) using a CT2001A cell test instrument (LAND Electronic Co.). The cyclic voltammetry (CV) measurement was conducted with a Gamry Reference 3000 electrochemical workstation at a scan rate of 0.2 mV s^{-1} in the voltage range of 1.7 to 3.0 V

(*vs.* Li/Li^+). Electrochemical impedance spectroscopy (EIS) was measured in the frequency range of 100 kHz-10 mHz with an amplitude of 5 mV.

Computational Section

The structural optimization was carried out by employing the Vienna ab initio Simulation Package (VASP),[1, 2] which is based on density functional theory (DFT) and the projected augmented wave (PAW) method. Generalized gradient approximation (GGA) in the form of Perdew-Burke-Ernzerhof (PBE)[3] was chosen as exchange correlation potential. The electron wave functions were expanded by a plane wave basis set with a cutoff energy of 400 eV. All structures were fully optimized until none of the forces exceeded 0.02 eV $Å^{-1}$. The adsorption energy (E_a) is defined as the difference between the total energy (E_{tot}) of Li_2S_n (n = 4, 2 and 1) on substrate and the energy sum of Li_2S_n ($E_{Li_2S_n}$) and substrate (E_{sub}):

$$E_a = E_{tot} - (E_{Li_2S_n} + E_{sub})$$

The molecular dynamics (MD) simulation for the lithium salt/polysulfide mixture was created by randomly placing 14 Li^+, 14 $TFSI^-$, and 1 Li_2S_4 molecules in the simulation box to match the F:S atomic ratio in the ACNTP after cycling (**Table S2**). After the structural optimization using conjugate gradient method, a simulation box with the size of 13.2×13.3×13.5 Å corresponding to 2.9 g cm^{-3} was obtained. The MD was performed at 298 K using velocity Verlet method with a time step of 1 fs. Following 1 ps of equilibration, 9 ps of the molecular dynamics trajectory was used to calculate the mean square displacement of the Li ions in the simulation cell and the S atoms in Li_2S_4.

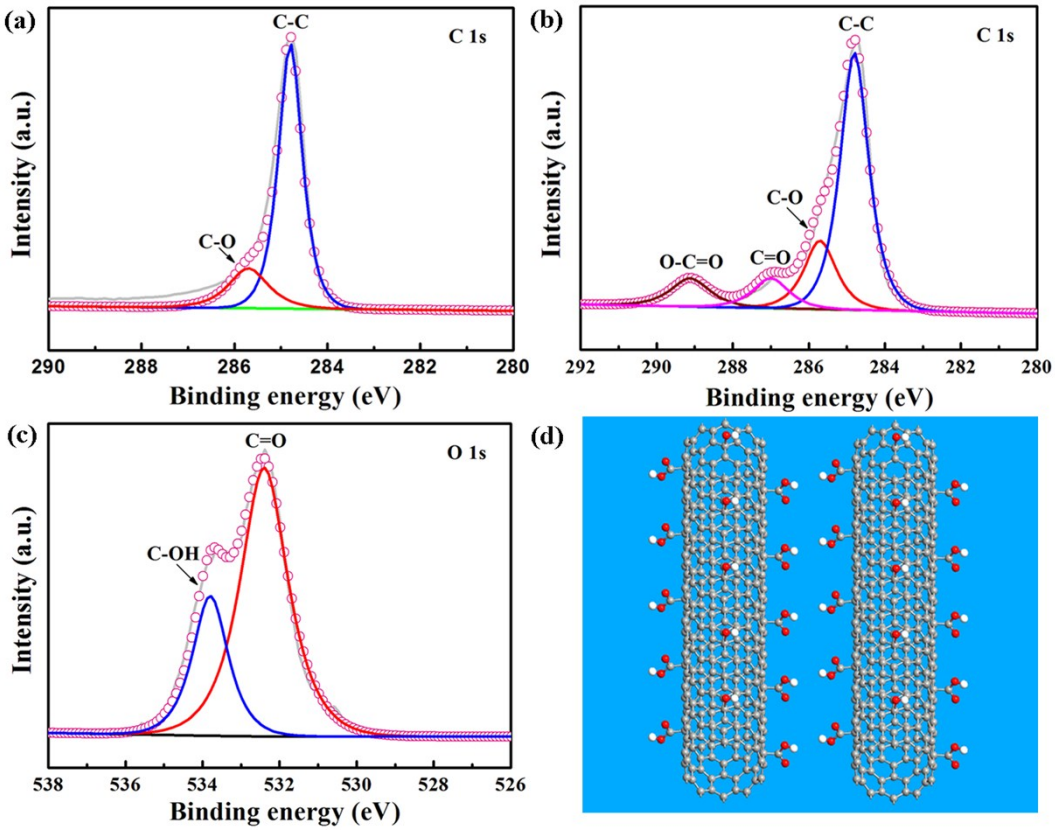

Figure S1. (a) C 1s X-ray photoelectron spectroscopy (XPS) spectra for CNTP. (b) C 1s and (c) O 1s XPS spectra for ACNTP. (d) Schematic illustration for the chemical structure of ACNTP. The gray, red and white balls in (d) represent C, O and H element, respectively.

XPS was carried out to analyze the carbon and oxygen bonds in CNTP and ACNTP. In the C 1s spectra of CNTP, the peak at 284.8 eV is attributed to the C-C bond (**Figure S1a)**. The peak at 285.7 eV corresponds to the C-O bond, which may result from the absorbed oxygen on the surface of CNTP. As shown in the C 1s spectra of ACNTP, the peaks at 289.1, 287.0, 285.7, 284.8 eV correspond to the O-C=O, C=O, C-O and C-C bonds, respectively (**Figure S1b**).[4, 5] In the O 1s spectra of ACNTP, the peaks at 533.8 and 532.5 eV are attributed to C-OH and C=O bonds (**Figure S1c**).[6] The results indicate the O–H and –COOH groups were successfully grafted onto ACNTP (**Figure S1d**).

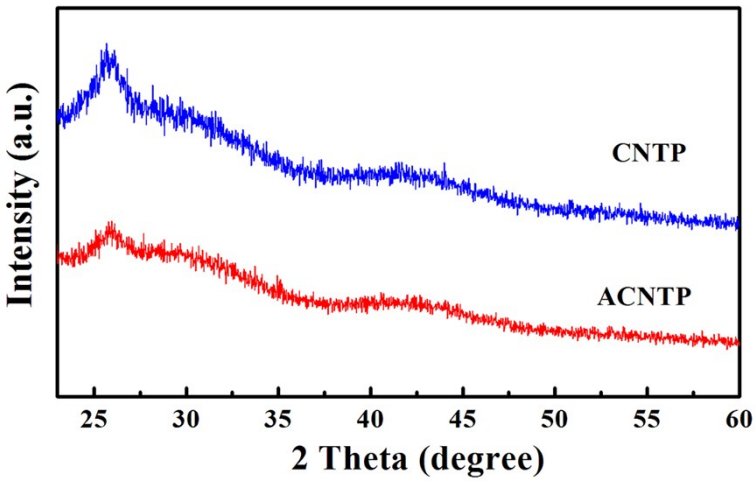

Figure S2. X-ray diffraction (XRD) patterns of CNTP and ACNTP. The peak intensity of ACNTP at about 26° and 42° decreased compared to that of CNTP in XRD patterns because the acid treatment broke the hexagonal symmetry of graphite lattice.[7]

Figure S3. Digital photographs of (a) CNTP, (b) ACNTP and (c) ACNTP after 250 cycles at 0.5 C. The flexibility of ACNTP remained after the nitric acid treatment.

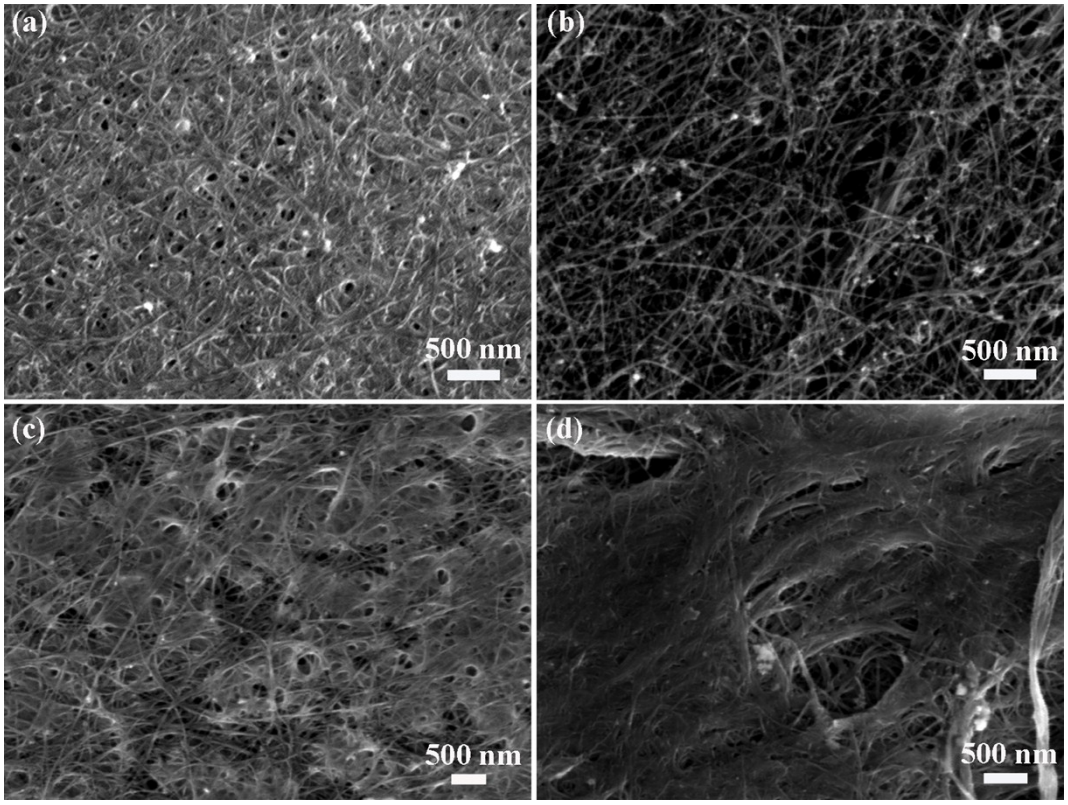

Figure S4. Scanning electron microscopy (SEM) images of (a) CNTP after dipped into the electrolyte, (b) CNTP after washing, (c) ACNTP after dipped into the electrolyte, and (d) ACNTP after washing.

The electrolyte can deposit on the surface of CNTP (**Figure S4a**). However, the electrolyte disappears after washed using absolute methanol (**Figure S4b**). The trapped electrolyte still deposits on the surface of ACNTP (**Figure S4c, d**), indicating the strong interaction between solvent molecules and the polar groups on ACNTP.

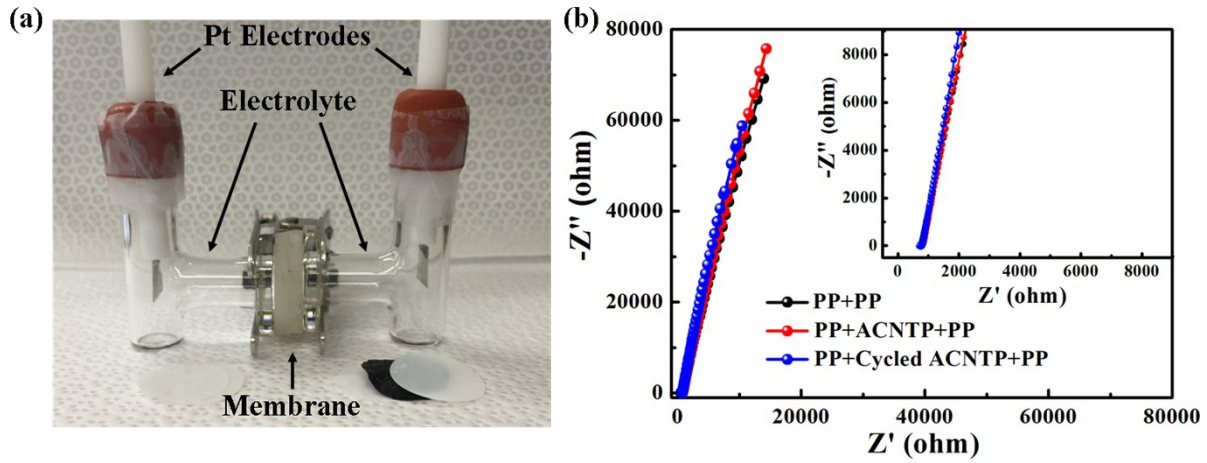

Figure S5. (a) Digital photograph of H-type cell. (b) Impedance plots of the H-type cell with different membranes in the electrolyte. The electrolyte is 1 mol L^{-1} LiTFSI and 0.1 mol L^{-1} $LiNO_3$ in a mixed solvent of 1, 3-dioxolane (DOL) and 1, 2-dimethoxyethane (DME) with a volume ratio of 1:1. The membranes are two-layer polypropylene separator (PP+PP), with the ACNTP barrier or the cycled ACNTP barrier placed in between (PP+ACNTP+PP, PP+Cycled ACNTP+PP).

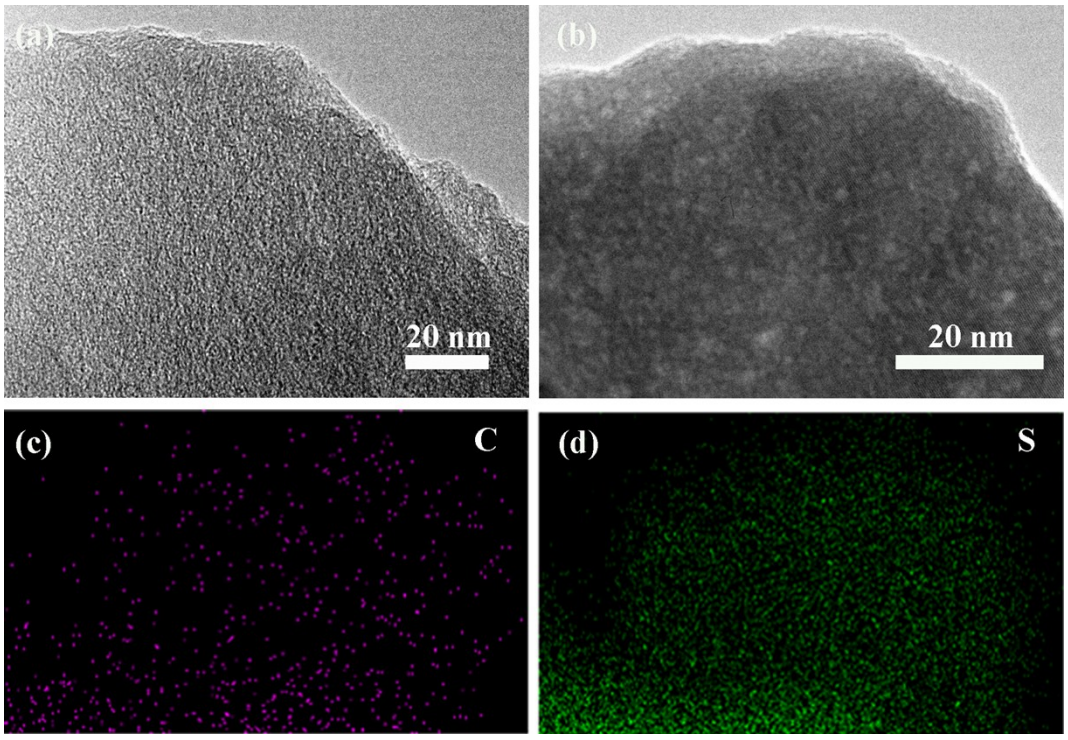

Figure S6. Transmission electron microscopy (TEM) image of (a) AC, (b) AC/S and the corresponding elemental mapping images for (c) carbon and (d) sulfur.

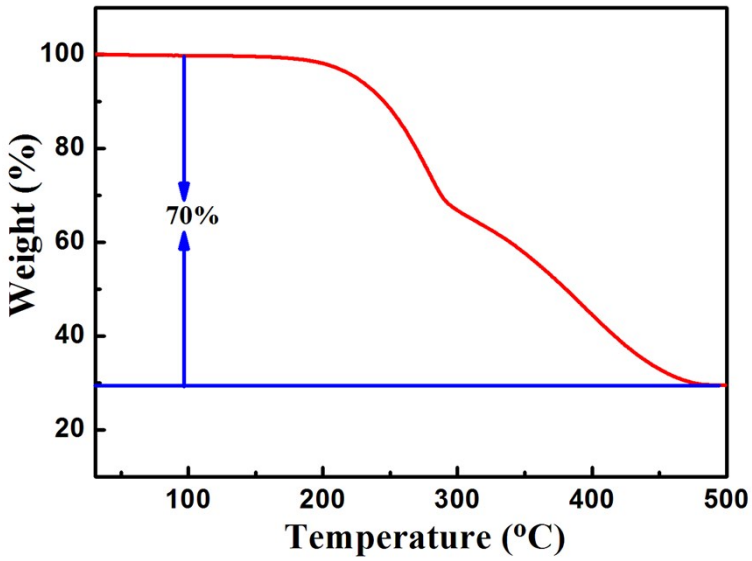

Figure S7. TG curve of the AC/S composite.

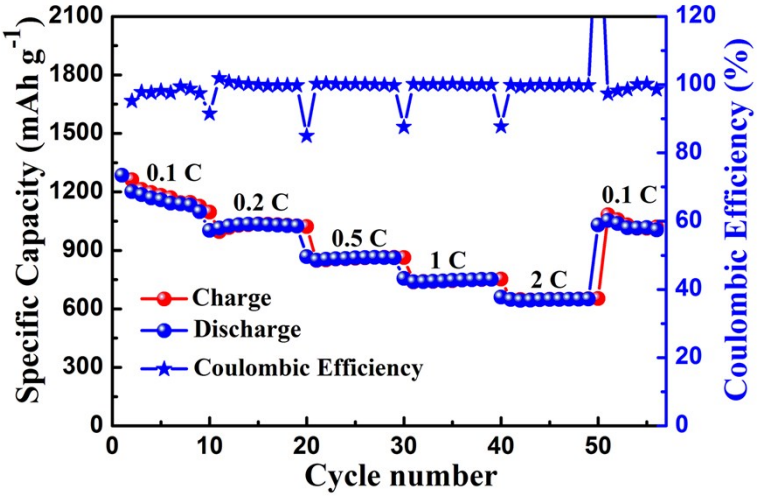

Figure S8. Rate capability of AC/S composite electrode with the ACNTP barrier.

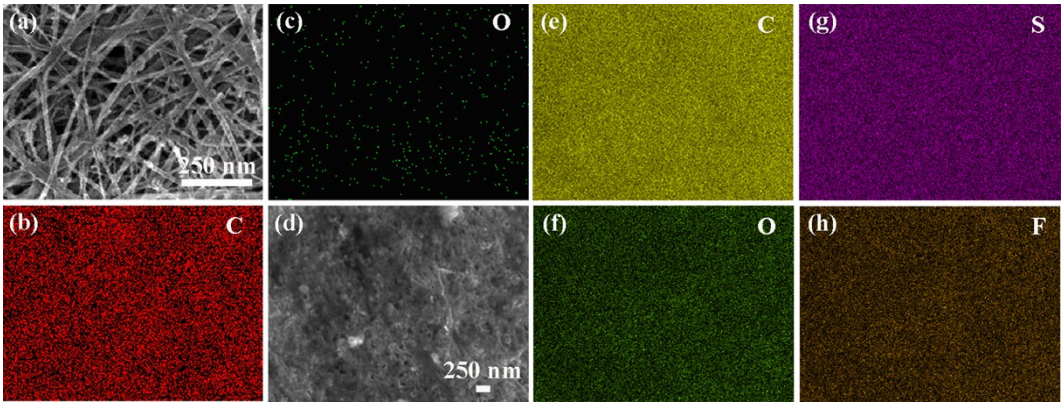

Figure S9. (a) Scanning electron microscopy (SEM) image of ACNTP and corresponding energy-dispersive X-ray spectroscopy (EDS) elemental maps of (b) carbon, (c) oxygen. SEM and EDS characterization of ACNTP after 50 cycles at 0.5 C (charged state): (d) SEM images of the cycled ACNTP. (e-h) EDS elemental maps for the region shown in (d): (e) carbon, (f) oxygen, (g) sulfur and (h) fluorine.

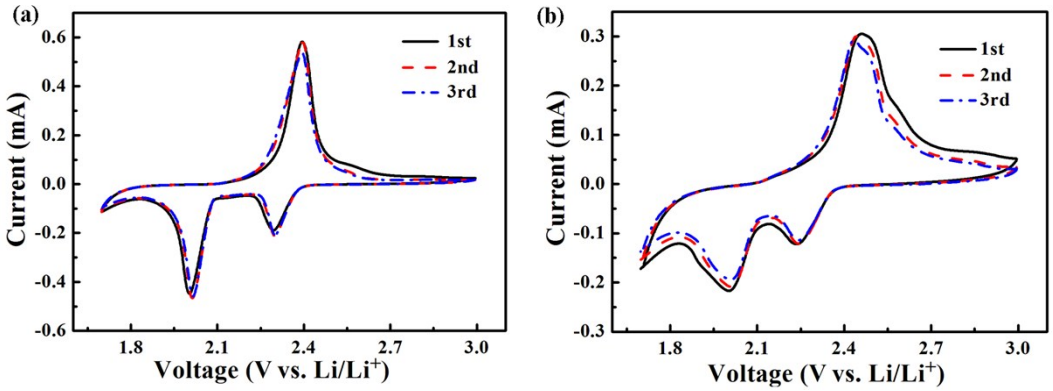

Figure S10. Typical cyclic voltammetry (CV) curves of (a) the CNTP barrier and (b) the ACNTP barrier as cathode after 50 cycles at 0.5 C.

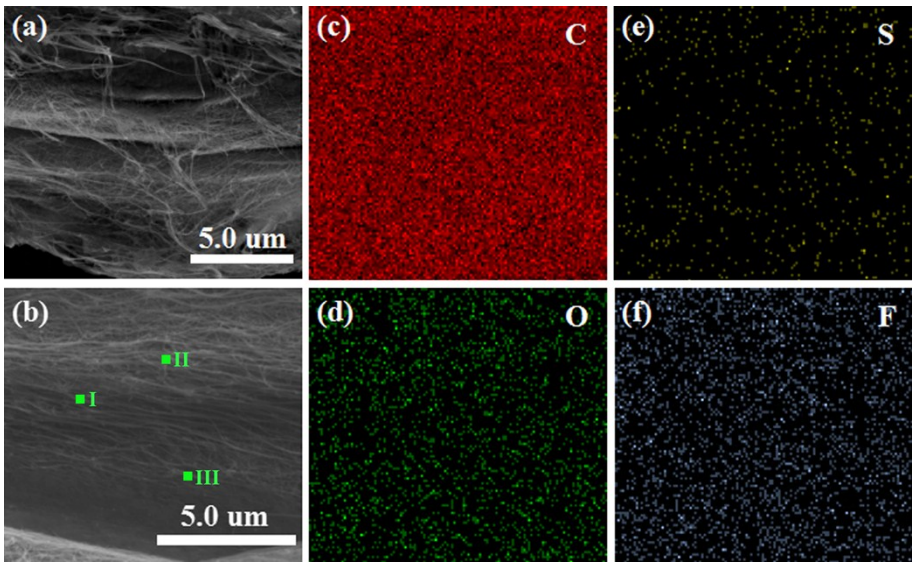

Figure S11. (a) Scanning electron microscopy (SEM) image of CNTP cross-section. SEM and EDS characterization of CNTP cross-section after 50 cycles at 0.5 C (charged state): (b) SEM images of the cycled CNTP cross-section. (c-f) EDS elemental maps for the region shown in (b): (c) carbon, (d) oxygen, (e) sulfur and (f) fluorine.

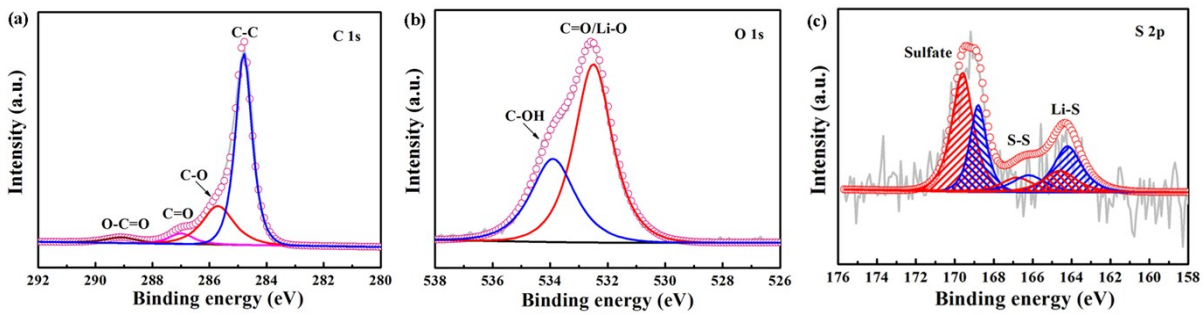

Figure S12. (a) C 1s, (b) O 1s, and (c) S 2p XPS spectra for ACNTP after 50 cycles at 0.5 C.

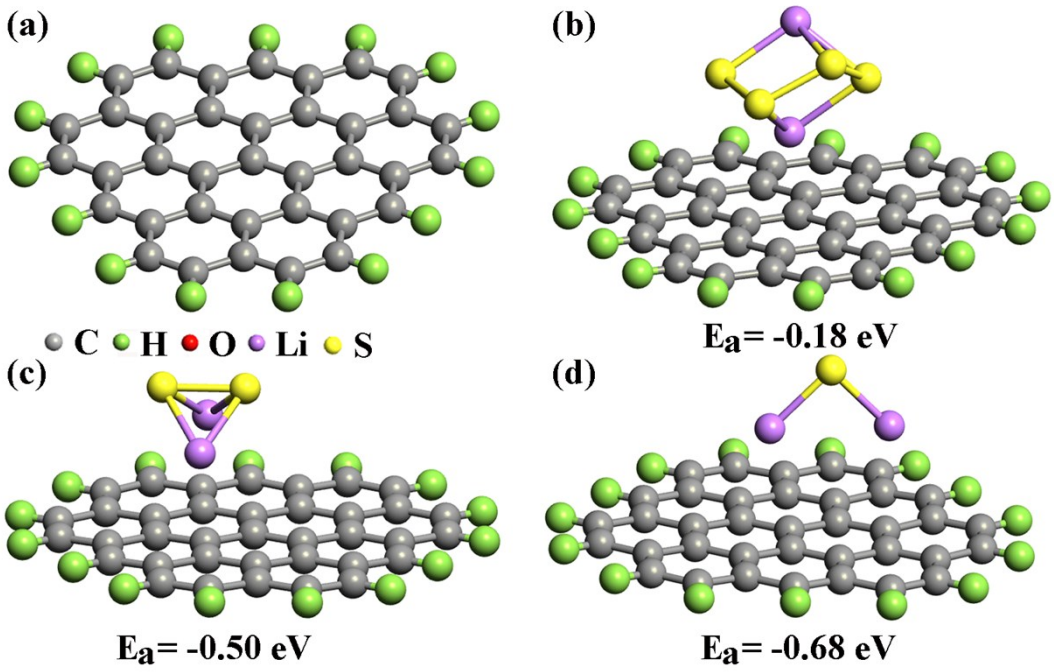

Figure S13. The representative geometries after fully optimized show the interactions between (a) the CNTP surface and (b-d) the Li_2S_n (n=4, 2, 1) molecules.

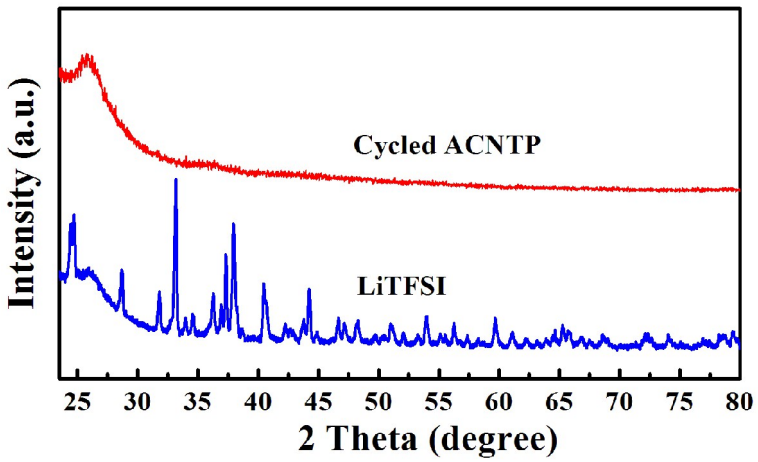

Figure S14. XRD patterns of cycled ACNTP and LiTFSI.

Table S1. The composition of cycled CNTP in **Figure S9**. The amounts of C, O, F, S (at. %) are estimated from EDS.

	I	II	III
C	98.04 %	97.27 %	97.89 %
O	1.01 %	1.48 %	0.77 %
F	0.63 %	0.92 %	0.98 %
S	0.33 %	0.33 %	0.35 %

Table S2. The composition of cycled ACNTP in **Figure 4**. The amounts of C, O, F, S (at. %) are estimated from EDS.

	I	II	III	IV
C	75.89 %	75.97 %	70.69 %	71.05 %
O	10.13 %	10.22 %	7.76 %	10.90 %
F	9.78 %	8.56 %	6.49 %	12.05 %
S	4.21 %	5.25 %	15.06 %	6.01 %

Video S1 and 2. The tension of the cycled ACNTP after 50 cycles at 0.5 C (Played at x5 original speed).

Video S3. The molecular dynamics simulation of the LiTFSI/Li_2S_4 mixture.

References

1 G. Kresse and J. Hafner, *Phys. Rev. B*, 1993, **47**, 558-561.

2 G. Kresse and J. Furthmüller, *Phys. Rev. B*, 1996, **54**, 11169-11186.

3 J. P. Perdew, K. Burke and M. Ernzerhof, *Phys. Rev. Lett.*, 1996, **77**, 3865-3868.

4 S. Stankovich, D. A. Dikin, R. D. Piner, K. A. Kohlhaas, A. Kleinhammes, Y. Jia, Y. Wu, S. T. Nguyen and R. S. Ruoff, *Carbon*, 2007, **45**, 1558-1565.

5 Y. Xu, K. Sheng, C. Li and G. Shi, *ACS Nano*, 2010, **4**, 4324-4330.

6 H. Gao, L. Song, W. Guo, L. Huang, D. Yang, F. Wang, Y. Zuo, X. Fan, Z. Liu, W. Gao, R. Vajtai, K. Hackenberg and P. M. Ajayan, *Carbon*, 2012, **50**, 4476-4482.

7 P. Hohenberg and W. Kohn, *Phys. Rev.*, 1964, **136**, B864-B871.